GSA Data Repository 2018397

Supplementary data for

Oceanic Origins of Continental Mantle Lithosphere

Andrea Servali[1] and Jun Korenaga[1]

[1]Department of Geology and Geophysics, Yale University, PO Box 208109, New Haven, CT 06520-8109

*Corresponding author: Andrea Servali (email: andrea.servali@yale.edu)

Surface geology of cratons:

The data set includes samples from Churchill Province, Kaapvaal, Tanzania, Northern and Southern China, North Atlantic, Slave, Siberian, Karelian, and Wyoming cratons. In what follows, we summarize notable geological and geochemical characteristics for each of these cratons.

The Kaapvaal Craton comprises of several Archean terranes stabilized and amalgamated mostly by the early Proterozoic (de Wit et al., 1992). The Eastern Terrane is dominated by Paleoarchean tonalite-trondhjemite-granodiorite (TTG) gneisses and greenstone belts, whereas the Western Terrane is composed of Mesoarchean granitic gneisses and unfoliated granitoids and greenstone belts (e.g., Griffin et al., 2004). The welding of the Eastern and Western terranes took place during the Mesoarchean (e.g., Carlson and Moore, 2004). Two additional major modifications occurred to the Kaapvaal continental lithosphere, one in the Paleoproterozoic coincident to the Bushveld layered intrusion, the other in the Neoproterozoic with the accretion of the Namaqua-Natal orogenic belt (Carlson and Moore, 2004). The Kaapvaal Craton is surrounded by the Namaqua-Natal Province and the Rehoboth Province, both of which accreted during the Paleoproterozoic (Janney et al, 2010).

Mantle xenoliths from the Tanzania region sample mantle beneath two distinct regions: the highly metamorphosed Dodoman belt (Manya et al, 2006) located within the Tanzania Craton, which is composed of early to mid-Archean terranes (Chesley et al., 1999), and the currently rifting Proterozoic Usagaran belt located east of the craton.

Eastern China is characterized by a complex terrane assemblage subdivided into North and South China Blocks, connected by the Qinling-Dabie-Sulu orogenic belt formed during their collision in the Mesozoic (Menzies et al., 2007). The South China Block encompasses the Archean to Paleoproterozoic Yangtze and the Paleoproterozoic to Mesoproterozoic Cathaysia blocks that amalgamated in the Neoproterozoic. The South China Block experienced extensive magmatism between Paleozoic and Cenozoic that resulted into major granitic and basaltic intrusions in the crystalline basement (Liu et al., 2012). The Northern China Block includes three regions: Westen and Eastern Blocks and the Trans-North China Orogen. The Western Block has been tectonically stable and its crust is characterized by Archean metasedimentary belts. Instead, the East Block consists of re-activated Archean continental lithosphere that contains two distinct mantle xenoliths age groups spanning Phanerozoic and Archean; their age gap occurred in a rapid transition between the Paleozoic and Mesozoic, but relevant tectonics is still debated (e.g. Menzies et al., 2007).

The bulk of the Archean North Atlantic Craton is located in southern Greenland, which is covered by mostly perennial glaciers. The western part of the craton mainly consists of Neo- to Mesoarchean TTG and granitoids intermixed by Eoarchean terranes (Witting et al., 2010). The Paleoproterozoic Nagssuqotidian Orogen bounds to the north the North Atlantic Craton and it consists of reworked Archean terrains (Bizzarro et al., 2003; Witting et al., 2008). The North

Atlantic Craton retains highly refractory and pristine Archean mantle xenoliths and close age correspondence between crust and mantle (Hanghøj et al., 2001; Pearson et al., 2014).

Similar to the Kaapvaal Craton, the Siberian Craton is underlain by a lithospheric mantle characterized by silica enrichment. The Siberian Craton is mostly covered by Paleozoic sediments, but exposed parts of Anabar and Aldan shields show Paleoarchean gneisses and granulites basement (Ionov et al., 2010). The majority of mantle xenoliths here presented were collected from the Udachnaya and Obnazhennaya kimberlite fields (Ionov et al., 2015).

The Karelian Craton is predominantly composed of greenstone belts and TTG gneisses dating around the Neoarchean with some interbedded Mesoarchean terranes. All mantle xenoliths were recovered from the Kaavi-Kuopio kimberlite group in proximity to the southwestern border of the Karelian craton. During the Paleoproterozoic the border of the craton experienced a rifting event that was eventually followed by accretionary tectonics. These tectonic processes are responsible for mantle metasomatism and overprinting of the shallow Archean continental mantle (Peltonen et al, 2006).

The Laurentian shield consists of an assemblage of numerous Archean and Proterozoic terranes that are surrounded by Phanerozoic margins. Our compilation focuses on data collected from the Churchill Province, the Slave Craton and the Wyoming Craton. The Churchill Province experienced extensive Paleoproterozoic reactivation and contains two regions of geologically distinct age groups, one characterized by Archean gneisses, greenstone belts and granitoids, the other by Proterozoic magmatic and metamorphic rocks, associated to large igneous provinces and to the Taltson-Thelon orogeny, respectively (Irvine et al, 2003). The Slave Craton displays a distinct transition in age from east to west; the eastern basement is dominated by Neoarchean greenstone belts and plutonic suites, and the western basement contains Mesoarchean rocks including outliers as old as the Eoarchean Acasta gneiss (Heaman and Pearson, 2010). Lastly, kimberlites from the Wyoming province sample three distinct tectonic areas, the Archean Wyoming Craton, the Paleoproterozoic Great Fall tectonic suture zone, and the closely dated Central Plains orogen.

Figure Captions:

Supplementary Figure DR1: Covariation of whole-rock Fo contents and model ages for mantle xenoliths from (a) Kaapvaal and Tanzania cratons, (b) China cratons, (c) North Atlantic craton, and (d) other major cratons. For the majority of data, both T_{RD} and T_{MA} ages are shown (with T_{MA} being older). Solid symbols denote T_{RD} model ages corrected for eruption contamination, whereas open symbols denote those uncorrected. Dark blue symbols connected with line denote data with T_{MA}-T_{RD} < 0.2 Gy. Light blue symbols are used for data with T_{MA}-T_{RD} < 1 Gy. Symbols connected by dashed line are used for data uncorrected for eruption contamination. Gray symbols represent T_{RD} ages, for data with T_{MA} more than 1 Gy apart from T_{RD}, or with only T_{RD} ages reported. Our coding of symbols is to place greater emphasis on more reliable data. Shown in pink shading is the range of Mg# corresponding to the thermal evolution model of Korenaga (2017) for three different values of Urey ratio. The parameterization of Herzberg and Rudnick (2012) is used to convert mantle potential temperature to the Mg# of mantle residue.

Supplementary Figure DR2: (a) Covariation of whole-rock Mg# and model ages for the global compilation of mantle xenoliths data. (b) Covariation of Fo contents and model ages for the global compilation of mantle xenoliths data. For the majority of data, both T_{RD} and T_{MA} ages are shown (with T_{MA} being older). Solid symbols denote T_{RD} model ages corrected for eruption contamination, whereas open symbols denote those uncorrected. Here the color coding of the symbols represents the rock types of mantle xenoliths (green: dunite, red: lherzolite, blue: harzburgite, brown: wehrlite, yellow: pyroxenite, gray: peridotites (unclassified)). As in Fig. DR1, predictions based on the thermal evolution model of Korenaga (2017) are also shown in both panels.

Supplementary Figure DR3: Comparison of T_{RD} ages computed with the estimates of primordial $^{187}Re/^{188}Os$ and $^{187}Os/^{188}Os$ according to Shirley and Walker (1998), Miesel et al. (2001), Brandon et al. (2001), and Walker et al. (2002). Dashed lines show differences between them; difference can be up to ~500 Myr for Phanerozoic model ages.

Supplementary Table: The table is organized by craton rather than by author or alphabetical order. From row 2 through 175 are for xenoliths from the Kaapvaal Craton and its surroundings, from row 176 through 194 are for theTanzania Craton, from row 195 through 376 are for China Blocks, from row 377 through 447 are for the North Atlantic Craton and its surroundings, from row 348 through 466 are for the Karelian Craton, from row 467 through 517are for the Siberian Craton, and from row 519 through 602 are those from the North American continent. The first five columns provide general information on sample: sample number, kimberlite in which it was collected, reference paper or papers, and the approximate location of the kimberlite. The next eleven columns contain major modal mineral composition and major oxide compositions in weight percent. Columns 17 and 18 are for equilibration temperature and pressure, respectively. Columns 19 is for whole-rock Mg#. Mg# is either computed using reported FeO and Fe_2O_3 by $(MgO \div 40.3044) \div ((MgO \div 40.3044) + ((FeO + Fe_2O_3 \times 0.8998) \div 71.844)) \times 100$ or, when iron oxide data is not readily available, it is reported as given by original publication. Column 20 includes data for Fo contents as reported by original publications. The next five columns (21-25) and column 29 contain information on whole-rock Re-Os concentrations as well as corresponding reported model ages by the authors of original analyses. Column 21 contains $^{187}Os/^{188}Os$ data, column 22 contains $^{187}Re/^{188}Os$ data, and columns 23 contains $^{187}Os/^{188}Os$ corrected for contamination during kimberlite eruption. Columns 24 and 25 list, respectively, T_{RD} and T_{MA} reported by authors, and column 29 shows the primordial $^{187}Re/^{188}Os$ and $^{187}Os/^{188}Os$ estimates adopted for model age calculations in columns 24 and 25. Columns 26 to 28 are for the rock types of mantle xenoliths. We report rock types either based on modal mineralogy or, when absent, according to rock type as reported by original publications. Nomenclature for rock type is as follow: G stands for garnet, S for spinel, H for harzburgite, L for lherzolite, Py for pyroxenite, P for peridotite, D for dunite, W for wehrlite. Columns 30-33 include model ages computed using T_{RD} and T_{MA} from Shirley and Walker (1998). Columns 30 and 31 are T_{RD} and T_{MA} recomputed for the values of primordial $^{187}Re/^{188}Os$ and $^{187}Os/^{188}Os$ estimates from original manuscript, whereas columns 32 and 33 contain recomputed primordial $^{187}Re/^{188}Os$ and $^{187}Os/^{188}Os$ estimates for primordial $^{187}Re/^{188}Os$ and $^{187}Os/^{188}Os$ values from Walker et al. (2002).

REFEENCES CITED

Becker, H., Horan, M.F., Walker, R.J., Gao, S., Lorand, J.P., Rudnick, R.L., 2006. Highly siderophile element composition of the Earth's primitive upper mantle: constraints from new data on peridotite massifs and xenoliths. Geochimica et Cosmochimica Acta, v. 70, p. 4528-4550.

Bizzarro, M. and Stevenson, R.K., 2003. Major element composition of the lithospheric mantle under the North Atlantic craton: evidence from peridotite xenoliths of the Sarfartoq area, southwestern Greenland. Contributions to Mineralogy and Petrology, v. 146, p. 223-240.

Brandon, A.D., Snow, J.E., Walker, R.J., Morgan, J.W., Mock, T.D., 2001. ^{190}Pt-^{186}Os and ^{187}Re-^{187}Os systematics of abyssal peridotites. Earth Planet Sci Lett, v. 177, p. 319-335.

Canil, D. and O'Neill, H.S.C., 1996. Distribution of ferric iron in some upper mantle assemblages. Journal of Petrology, v. 37, p. 609-635.

Carlson, R.W. and Moore, R.O., 2004. Age of the Eastern Kaapvaal mantle: Re-Os isotope data for peridotite xenoliths from the Monastery kimberlite. South African Journal of Geology, v. 107, p. 81-90.

Carlson, R.W., Irving, A.J., Schulze, D.J. and Hearn, B.C., 2004. Timing of Precambrian melt depletion and Phanerozoic refertilization events in the lithospheric mantle of the Wyoming Craton and adjacent Central Plains Orogen. Lithos, v. 77, p. 453-472.

Chesley, J.T., Rudnick, R.L. and Lee, C.T., 1999. Re-Os systematics of mantle xenoliths from the East African Rift: Age, structure, and history of the Tanzanian craton. Geochimica et Cosmochimica Acta, v. 63, p. 1203-1217.

Chu, Zhu-Yin,, Wu, Fu-Yuan., Walker, R.J., Rudnick, R.L., Pitcher, L., Puchtel, I.S., Yang, Yue-Heng. and Wilde, S.A., 2009. Temporal evolution of the lithospheric mantle beneath the eastern North China Craton. Journal of Petrology, v. 50, p. 1857-1898.

de Wit, M.J., de Ronde, C.E., Tredoux, M., Roering, C., Hart, R.J., Armstrong, R.A., Green, R.W., Peberdy, E. and Hart, R.A., 1992. Formation of an Archaean continent. Nature, v. 357, p. 553-562.

Doucet, L.S., Ionov, D.A., Golovin, A.V. and Pokhilenko, N.P., 2012. Depth, degrees and tectonic settings of mantle melting during craton formation: inferences from major and trace element compositions of spinel harzburgite xenoliths from the Udachnaya kimberlite, central Siberia. Earth and Planetary Science Letters, v. 359, p. 206-218.

Doucet, L.S., Ionov, D.A. and Golovin, A.V., 2013. The origin of coarse garnet peridotites in cratonic lithosphere: new data on xenoliths from the Udachnaya kimberlite, central Siberia. Contributions to Mineralogy and Petrology, v. 165, p. 1225-1242.

Gao, Shan, Rudnick, R.L., Carlson, R.W., McDonough, W.F. and Liu, Yong-Sheng, 2002. Re–Os evidence for replacement of ancient mantle lithosphere beneath the North China craton. Earth and Planetary Science Letters, v. 198, p. 307-322.

Griffin, W.L., Graham, S., O'Reilly, S.Y. and Pearson, N.J., 2004. Lithosphere evolution beneath the Kaapvaal Craton: Re–Os systematics of sulfides in mantle-derived peridotites. Chemical Geology, v. 208, p. 89-118.

Hanghøj, K., P. Kelemen, S. Bernstein, J. Blusztajn, and R. Frei, 2001, Osmium isotopes in the Wiedemann Fjord mantle xenoliths: A unique record of cratonic mantle formation by melt depletion in the Archaean, Geochem. Geophys. Geosyst., v. 2, 1011, doi: 10.1029/2000GC000085.

Heaman, L.M. and Pearson, D.G., 2010. Nature and evolution of the Slave Province subcontinental lithospheric mantle. This article is one of a series of papers published in this Special Issue on the theme Lithoprobe parameters, processes, and the evolution of a continent. Canadian Journal of Earth Sciences, v. 47, p. 369-388.

Herzberg, C. and Rudnick, R., 2012. Formation of cratonic lithosphere: an integrated thermal and petrological model. Lithos, v. 149, p. 4-15.

Ionov, D.A., Carlson, R.W., Doucet, L.S., Ashchepkov I.V., 2010. Composition of the Lithospheric Mantle in the Siberian Craton: New constraints from fresh peridotites in the Udachnaya-East Kimberlite. Journal of Petrology, v. 51, p. 2177-2210.

Ionov, D.A., Carlson, R.W., Doucet, L.S., Golovin, A.V. and Oleinikov, O.B., 2015a. The age and history of the lithospheric mantle of the Siberian craton: Re–Os and PGE study of peridotite xenoliths from the Obnazhennaya kimberlite. Earth and Planetary Science Letters, v. 428, p. 108-119.

Ionov, D.A., Doucet, L.S., Carlson, R.W., Golovin, A.V. and Korsakov, A.V., 2015b. Post-Archean formation of the lithospheric mantle in the central Siberian craton: Re–Os and PGE study of peridotite xenoliths from the Udachnaya kimberlite. Geochimica et Cosmochimica Acta, v. 165, p. 466-483.

Irvine, G.J., 2001. The Slave Craton-peridotite xenoliths from the Jericho Kimberlite. [Ph.D.thesis]: University of Durham, p. 142-227.

Irvine, G.J., Pearson, D.G., Kjarsgaard, B.A., Carlson, R.W., Kopylova, M.G. and Dreibus, G.,2003. A Re–Os isotope and PGE study of kimberlite-derived peridotite xenoliths from Somerset Island and a comparison to the Slave and Kaapvaal cratons. Lithos, v. 71, p. 461-488.

Janney, P.E., Shirey, S.B., Carlson, R.W., Pearson, D.G., Bell, D.R., Le Roex, A.P., Ishikawa, A., Nixon, P.H. and Boyd, F.R., 2010. Age, composition and thermal characteristics of South African off-craton mantle lithosphere: Evidence for a multi-stage history. Journal of Petrology, v. 51, p. 1849-1890.

Kopylova, M.G. and Russell, J.K., 2000. Chemical stratification of cratonic lithosphere: constraints from the Northern Slave craton, Canada. Earth and Planetary Science Letters, v. 181, p. 71-87.

Korenaga, J., 2017. Pitfalls in modeling mantle convection with internal heat production. Journal of Geophysical Research Solid Earth, v. 122, p. 4064-4085, doi:10.1002/2016JB013850.

Liu, Jingao, Rudnick, R.L., Walker, R.J., Gao, Shan, Wu, Fuyuan. and Piccoli, P.M., 2010. Processes controlling highly siderophile element fractionations in xenolithic peridotites and their influence on Os isotopes. Earth and Planetary Science Letters, v. 297, p. 287-297.

Liu, Chuan-Zhou., Liu, Zhi-Chao., Wu, Fu-Yuan and Chu, Zhu-Yin, 2012. Mesozoic accretion of juvenile sub-continental lithospheric mantle beneath South China and its implications: Geochemical and Re–Os isotopic results from Ningyuan mantle xenoliths. Chemical Geology, v. 291, p.186-198.

Manya, S., Kobayashi, K., Maboko, M.A. and Nakamura, E., 2006. Ion microprobe zircon U–Pb dating of the late Archaean metavolcanics and associated granites of the Musoma-Mara Greenstone Belt, Northeast Tanzania: Implications for the geological evolution of the Tanzania Craton. Journal of African Earth Sciences, v. 45, p. 355-366.

Meisel, T., Walker, R.J., Irving, A.J. and Lorand, J.P., 2001. Osmium isotopic compositions of mantle xenoliths: a global perspective. Geochimica et Cosmochimica Acta, v. 65, p.1311-1323.

Menzies, M., Xu, Y., Zhang, H. and Fan, W., 2007. Integration of geology, geophysics and geochemistry: a key to understanding the North China Craton. Lithos, v. 96, p. 1-21.

Pearson, D.G., Carlson, R.W., Shirey, S.B., Boyd, F.R. and Nixon, P.H., 1995. The Stabilisation of Archaean lithospheric mantle: A Re Os isotope study of peridotite xenoliths from the Kaapvaal craton. Earth and Planetary Science Letters, v. 134, p. 341-357.

Pearson, D.G., Wittig, N., 2014. The Formation and Evolution of Cratonic Mantle Lithosphere – Evidence from Mantle Xenoliths. In Treatise on Geochemistry (Second Edition), v. 3, p. 255-292.

Peltonen, P. and Brügmann, G., 2006. Origin of layered continental mantle (Karelian craton, Finland): geochemical and Re–Os isotope constraints. Lithos, v. 89, p. 405-423.

Rudnick, R.L., Gao, Shan, Ling, Wen-li, Liu, Yong-shen and McDonough, W.F., 2004. Petrology and geochemistry of spinel peridotite xenoliths from Hannuoba and Qixia, North China craton. Lithos, v. 77, p. 609-637.

Sand, K.K., Waight, T.E., Pearson, D.G., Nielsen, T.F., Makovicky, E. and Hutchison, M.T., 2009. The lithospheric mantle below southern West Greenland: A geothermobarometric approach to diamond potential and mantle stratigraphy. Lithos, v. 112, p. 1155-1166.

Shirey, S.B. and Walker, R.J., 1998. The Re-Os isotope system in cosmochemistry and high temperature geochemistry. Annual Review of Earth and Planetary Sciences, v. 26, p 423-500.

Simon, N.S., Carlson, R.W., Pearson, D.G. and Davies, G.R., 2007. The origin and evolution of the Kaapvaal cratonic lithospheric mantle. Journal of Petrology, v. 48, p. 589-625.

Walker, R.J., Carlson, R.W., Shirey, S.B. and Boyd, F.R., 1989. Os, Sr, Nd, and Pb isotope systematics of southern African peridotite xenoliths: implications for the chemical evolution of subcontinental mantle. Geochimica et Cosmochimica Acta, v. 53, p. 1583-1595.

Walker, R.J., Horan, M.F., Morgan, J.W., Becker, H., Grossman, J.N. and Rubin, A.E., 2002. Comparative ^{187}Re-^{187}Os systematics of chondrites: Implications regarding early solar system processes. Geochimica et Cosmochimica Acta, v. 66, p. 4187-4201.

Wittig, N., Pearson, D.G., Webb, M., Ottley, C.J., Irvine, G.J., Kopylova, M., Jensen, S.M. and Nowell, G.M., 2008. Origin of cratonic lithospheric mantle roots: A geochemical study of peridotites from the North Atlantic Craton, West Greenland. Earth and Planetary Science Letters, v. 274, p. 24-33.

Wittig, N., Webb, M., Pearson, D.G., Dale, C.W., Ottley, C.J., Hutchison, M., Jensen, S.M. and Luguet, A., 2010. Formation of the North Atlantic Craton: Timing and mechanisms constrained from Re–Os isotope and PGE data of peridotite xenoliths from SW Greenland. Chemical Geology, v. 276, p. 166-187.

Xu, Yi-Gang, Blusztajn, J., Ma, Jin-Long, Suzuki, K., Liu, J.F. and Hart, S.R., 2008. Late Archean to Early Proterozoic lithospheric mantle beneath the western North China craton: Sr–Nd–Os isotopes of peridotite xenoliths from Yangyuan and Fansi. Lithos, v. 102, p.25-42.

Zhang, Hong-Fu, Goldstein, S.L., Zhou, Xin-Hua, Sun, Min, Zheng, Jian-Ping and Cai, Yue,2008. Evolution of subcontinental lithospheric mantle beneath eastern China: Re–Os isotopic evidence from mantle xenoliths in Paleozoic kimberlites and Mesozoic basalts. Contributions to Mineralogy and Petrology, v. 155, p. 271-293.

Table DR1. Data and sources for all cratons

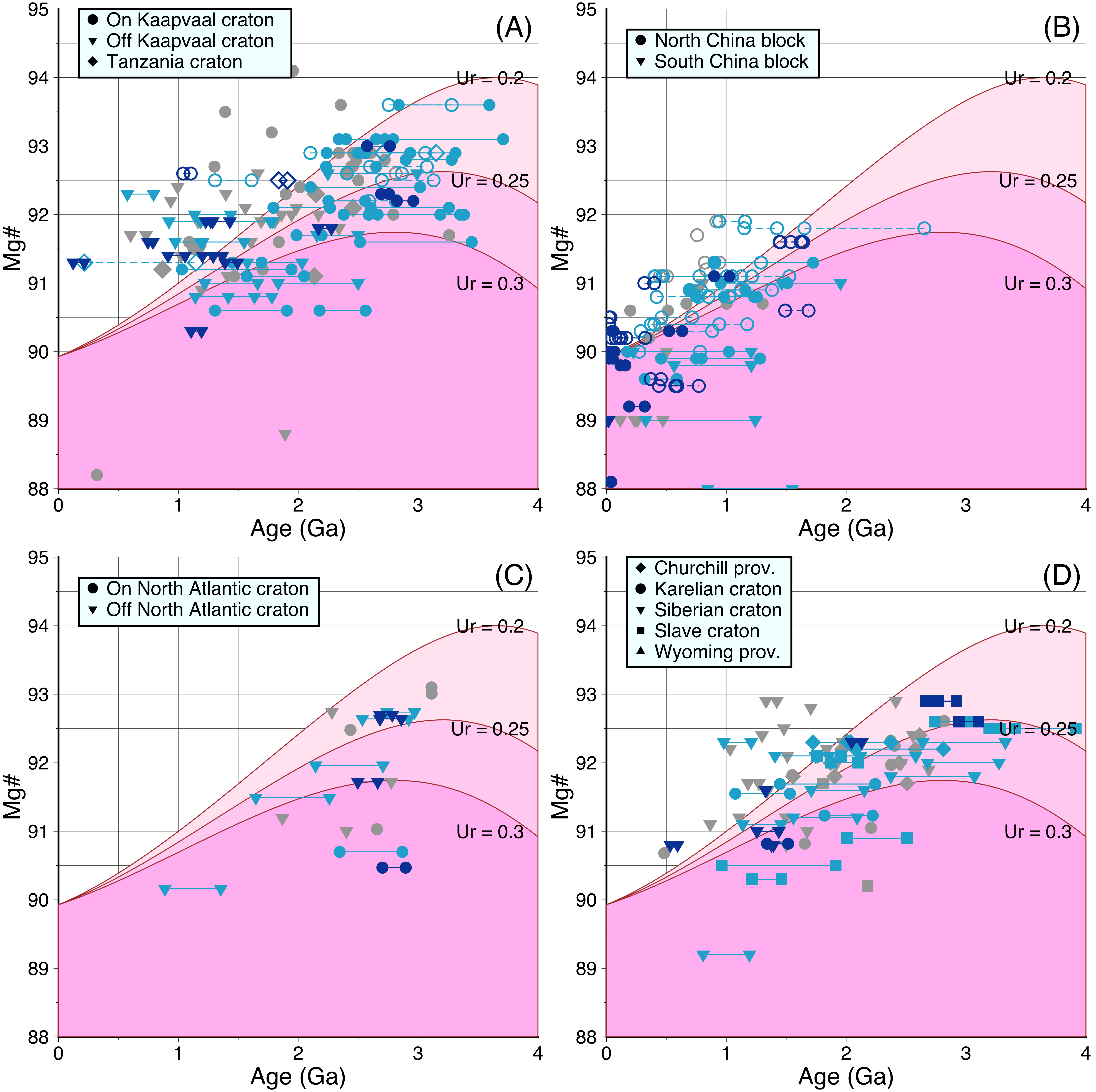

(A)
On Kaapvaal craton
Off Kaapvaal craton
Tanzania craton
(B)
North China block
South China block
(C)
On North Atlantic craton
Off North Atlantic craton
(D)
Churchill prov.
Karelian craton
Siberian craton
Slave craton
Wyoming prov.
Ur = 0.2
Ur = 0.25
Ur = 0.3
Mg#
Age (Ga)

Figure 1

Figure 2

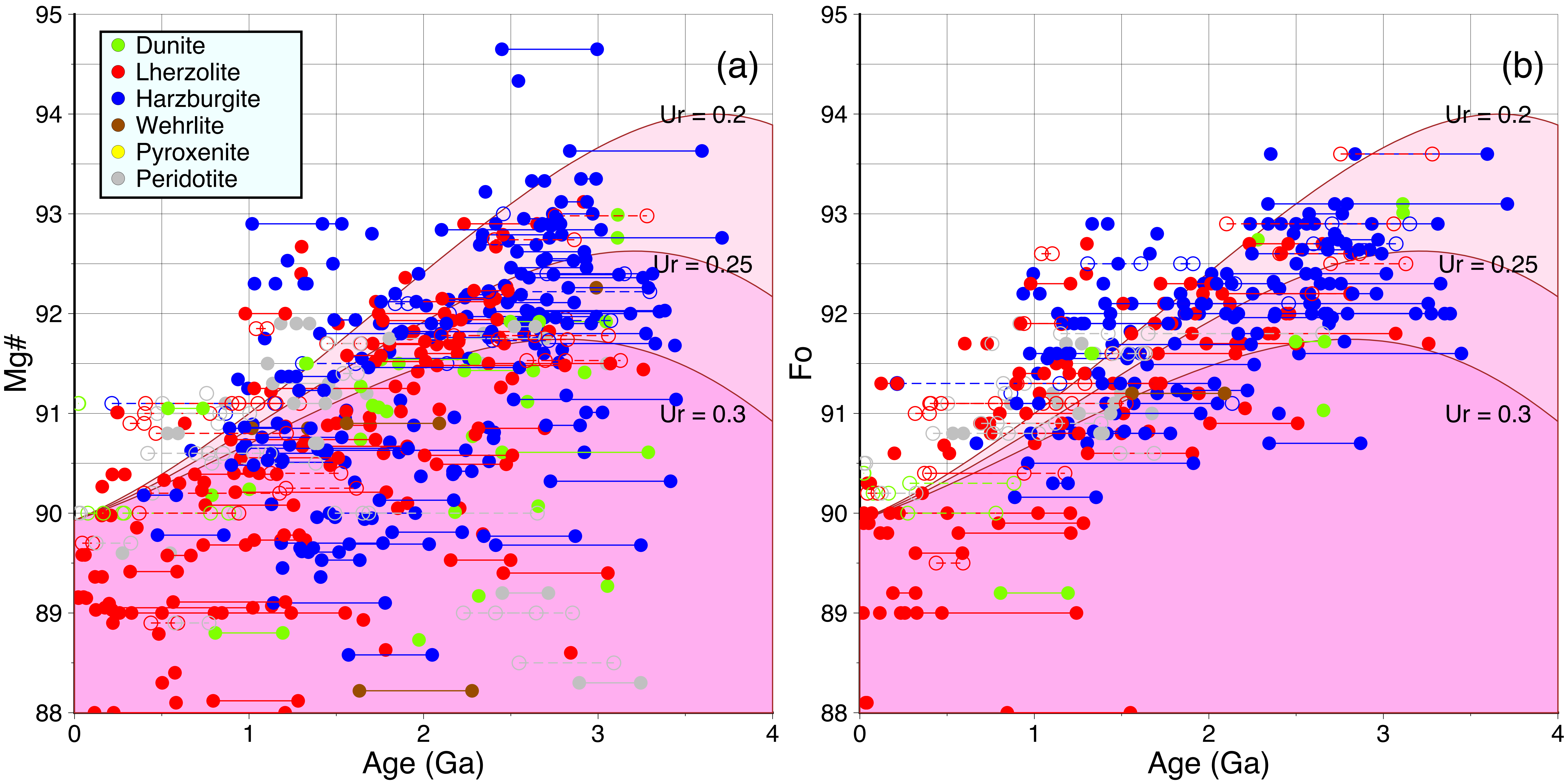

(a)
Dunite
Lherzolite
Harzburgite
Wehrlite
Pyroxenite
Peridotite
Ur = 0.2
Ur = 0.25
Ur = 0.3
Mg#
Age (Ga)
(b)
Ur = 0.2
Ur = 0.25
Ur = 0.3
Fo
Age (Ga)

Figure 3

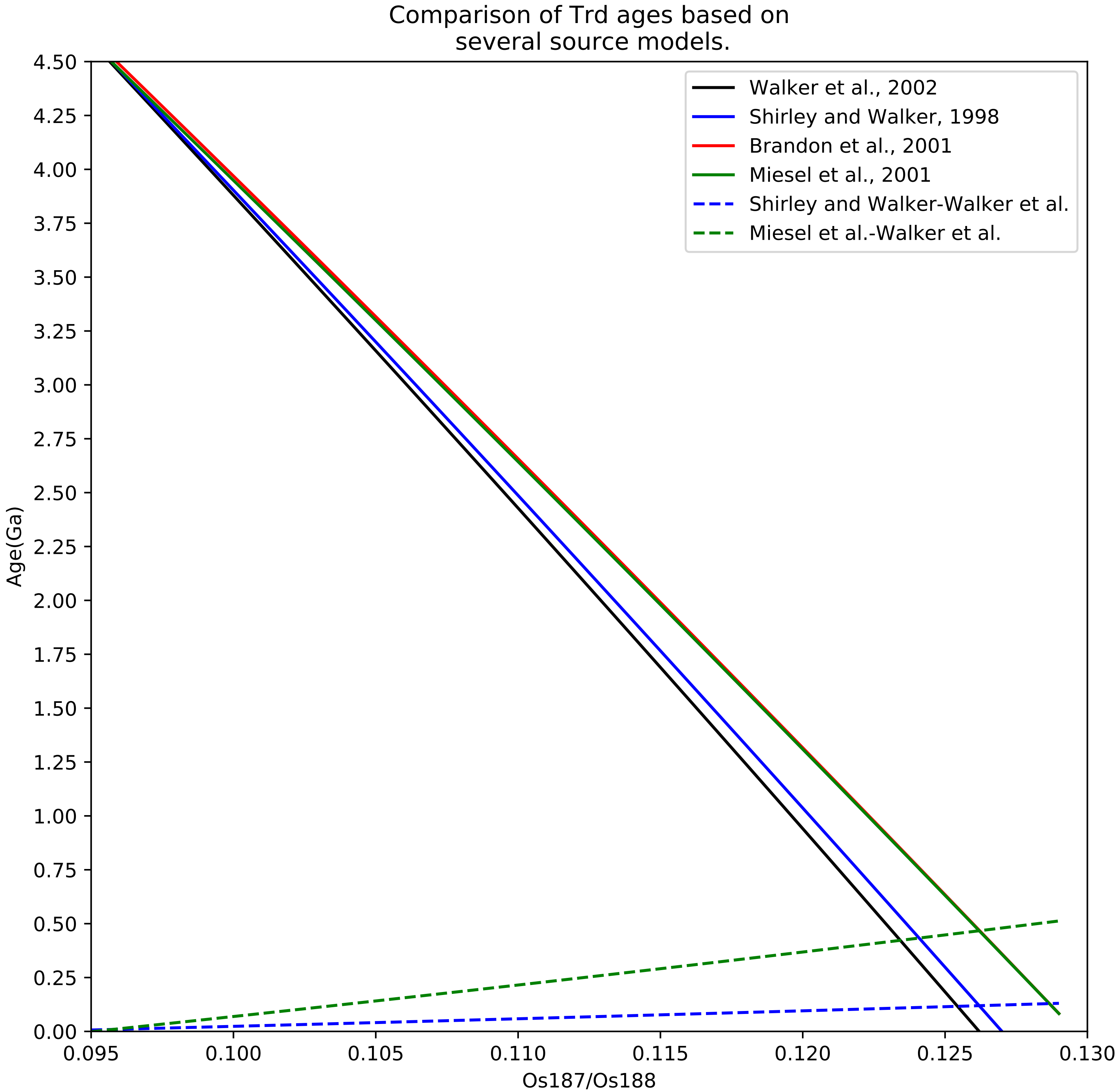

Comparison of Trd ages based on
several source models.
Walker et al., 2002
Shirley and Walker, 1998
Brandon et al., 2001
Miesel et al., 2001
Shirley and Walker-Walker et al.
Miesel et al.-Walker et al.
Age(Ga)
Os187/Os188
4.50
4.25
4.00
3.75
3.50
3.25
3.00
2.75
2.50
2.25
2.00
1.75
1.50
1.25
1.00
0.75
0.50
0.25
0.00
0.095
0.100
0.105
0.110
0.115
0.120
0.125
0.130